Electronic Supplementary Information

Ligand-mediated strategy for fabrication of hollow Fe-based MOFs and their derived Fe/NC nanostructures with enhanced oxygen reduction reaction

Yan Liu,[a] Yamin Zheng,[a] Panpan Dong,[a] Ning Lu,[a] Ruirui Zhang[b] and Junjie Mao*[a]

[a]Key Laboratory of Functional Molecular Solids, Ministry of Education, Anhui Province Key Laboratory of Optoelectric Materials Science and Technology, Anhui Normal University, Wuhu, 241002, China. E-mail: maochem@ahnu.edu.cn

[b]Department of Chemistry, Chair of Inorganic and Metal-Organic Chemistry, Technical University of Munich, 85748 Garching, Germany.

1. Experimental methods and characterizations

1.1 Reagents.

Ferric chloride hexahydrate, terephthalic acid (98.0 %), dimethylformamide, hexamethylenetetramine (99.0 %), ethanol and hydrochloric acid (38.0-40.0 %) were obtained from Sinopharm Chemical. In all of the experiments, the deionized water was obtained through ion-exchange and filtration. All the reagents were utilized without further purification.

1.2 Synthesis.

Synthesis of Fe-MOF：

Normally, 296 mg ferric chloride and 200 mg terephthalic acid were dissolved in the mixed solution of 20 ml DMF and 6 ml ethanol under vigorous stirring. After stirring for 30 minutes at room temperature, the mixture was transferred into 50 mL Teflon-lined stainless-steel autoclave, placed in an oven and heated at 150 ℃ for 3 h. After cooling down to room temperature， the Fe-MOF were obtained by centrifugation and washed with ethanol for several times.

Synthesis of Fe-MOF with hollow octahedral morphology:

Normally, 100 mg Fe-MOF and 200 mg Hexamethylenetetramine were dissolved in 30ml ethanol under vigorous stirring. After stirring for 30 minutes, the mixture was transferred into 50 mL Teflon-lined stainless-steel autoclave, and placed in an oven and heated at 170 ℃ for 20 h. After cooling down to room temperature，the hollow Fe-MOF were collected by centrifugation and washed with ethanol for several times.

Synthesis of o-Fe/NC:

Firstly, hollow octahedral shaped Fe-MOF was pyrolyzed at 900 ℃ under N_2 atmosphere for 3 h. After colling to room temperature, the above sample was treated with1 M HCl solution and stirring for 10 h to remove unstable Fe species.

1.3 Morphology analysis.

The morphology of the samples was characterized by transmission electron microscope (TEM) was operated by a Hitachi-7700 working at 100 kV. The HAADF-STEM images were obtained by FEI Tecnai G2 F20 S-Twin HRTEM which worked at 200 kV. HAADF-STEM images were obtained by using a Titan Cubed Themis 60–300 scanning transmission electron microscope operated at 300 kV, equipped with a probe spherical aberration corrector. The metal content of single atom catalysts was characterized by inductively coupled plasma-mass spectrometry (ICP-MS), which was carried out on Thermo Fisher IRIS Intrepid Ⅱ. Powder X-ray diffraction pattern (PXRD) was used a Rigaku D/max 2500Pc X-ray powder diffractometer with monochromatized Cu Kα radiation (λ =1.5418 Å).

1.4 Electrochemical measurements.

The ORR performance was measured by CHI760E electrochemical station with three-electrode system in 0.1 M KOH solution. Catalyst ink was preapared by 10 mg of catalyst ultrasonically dispersed into the mixture (2 mL) of ethanol (0.990 mL), water (0.990 mL) and Nafion solution (20 μL) for 30 min. Then 20 μL of the catalyst suspension was dropped on a fresh glassy carbon (GC) electrode. The substrate for the working electrode employed a rotating disk electrode (RDE) along with 5 mm diameter of GC disk. A graphite rod and Ag/AgCl electrode were selected as the counter electrode and reference electrode, respectively. The cyclic voltammetry (CV) tests were performed in O_2-saturated 0.1 M KOH solution with a scan rate of 50 mV s^{-1}. The linear sweep voltammetry (LSV) experiments were determined using RDE tests (1600 rpm). For further determine the long-term durability, the accelerated durability test was conducted with continuously cycling between 0.6 and 1.0 V vs. RHE in O_2-saturated 0.1 M KOH solution. Moreover, the tolerance to CH_3OH was verified by cyclic voltammetry measurements in O_2-saturated 0.1 M KOH solution.

1.5 Calculation details.

All the density functional theory (DFT) calculations were performed in the Vienna ab initio simulation package (VASP)[1]. Perdew-Burke-Ernzerhof (PBE)[2] exchange-correlation functional and projector augmented-wave (PAW)[3] potential were employed to describe electronic exchange-correlation effect and electron-ion interaction, respectively. The force and energy convergence criterion were set to be 0.02 eV/Å and 10^{-5} eV, respectively. The energy cutoff of 500 eV was employed for the plane wave expansion and a 15 Å vacuum region was constructed to avoid interactions between adjacent images. The Brillouin zone was sampled by 3×3×1 k-meshs in the Monkhorst-Pack[4] scheme. The overpotential for the ORR was calculated by the computational hydrogen electrode model[5]. The Gibbs-free-energy change (ΔG) of each oxygen reduction reaction (ORR) step was computed by the following equation:

$$\Delta G=\Delta E+\Delta ZPE-T\Delta S+\Delta G_U+\Delta G_{pH}$$

Where ΔE is the energy change, ΔZPE and ΔS is the zero point energy and entropy change at 298.15 K, respectively. $\Delta G_U = -eU$ represents the devotion from an electron transferring at the electrode potential U. $\Delta G_{pH} = kBTln10 \times pH$ is the contribution of the hydrogen ion. U and pH are set to be 0.

The overall reaction of O_2 reduction to H_2O in acidic environment is a four-electron reaction: $O_2 + 4H^+ + 4e^- \rightarrow 4H_2O$, which is divided into the following four fundamental steps:

(1) $* + O_2(g) + H^+ + e^- \rightarrow *OOH$

(2) $*OOH + H^+ + e^- \rightarrow *O + H_2O(l)$

(3) $*O + H^+ + e^- \rightarrow *OH$

(4) $*OH + H^+ + e^- \rightarrow H_2O(l) + *$

* represents the adsorption site.

The overpotential (η), a critical parameter of the ORR activity, is defined as η=1.23 eV−|ΔGmin|/e, where ΔGmin is the minimum Gibbs free energy of the four reactions above.

2. Supplementary Figures

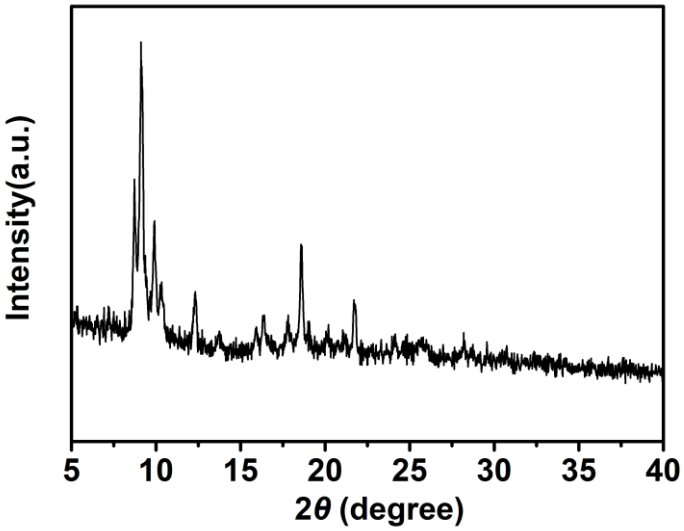

Figure S1. PXRD patterns of the Fe-MOFs.

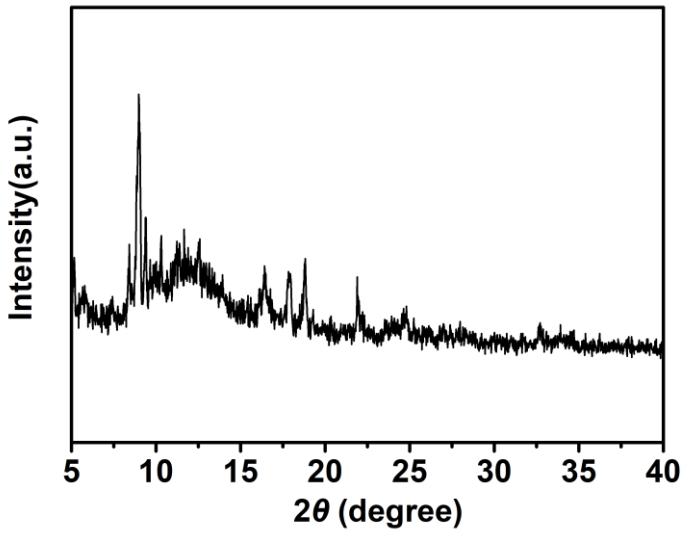

Figure S2. PXRD patterns of the hollow Fe-MOFs.

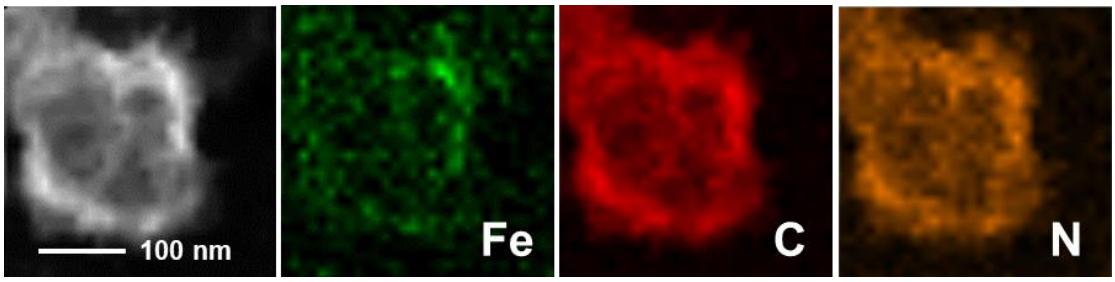

Figure S3. HAADF-STEM image and corresponding EDS element mapping images of the o-Fe/NC

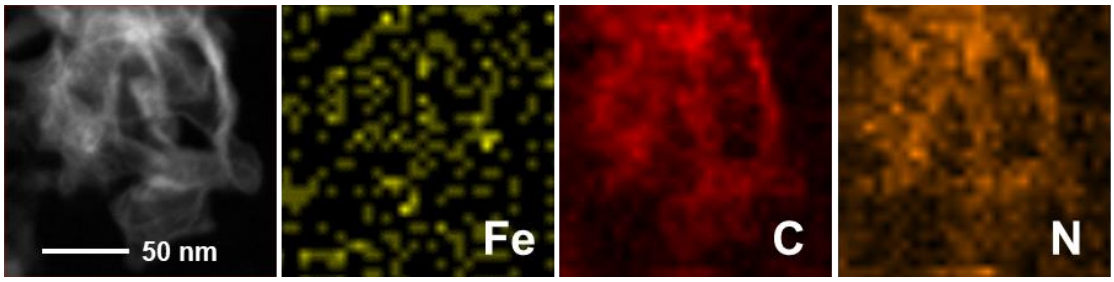

Figure S4. HAADF-STEM image and corresponding EDS element mapping images of Fe/NC.

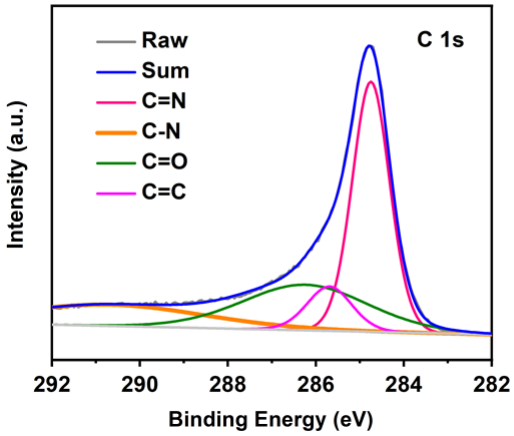

Figure S5. The XPS spectrum of C1s for the o-Fe/NC.

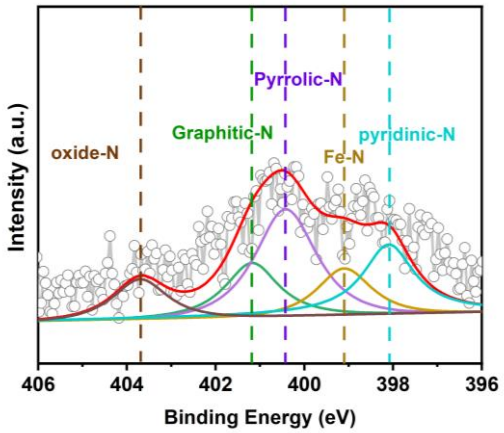

Figure S6. The XPS spectrum of N1s for the m-Fe/NC.

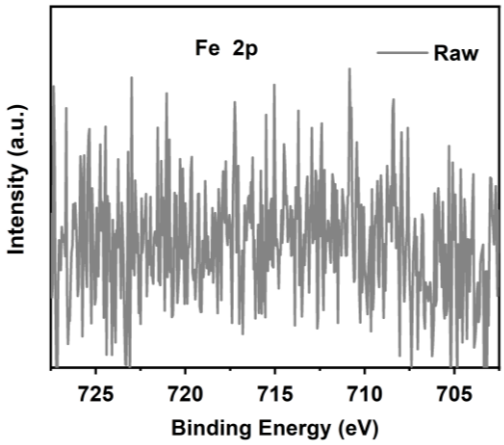

Figure S7. The XPS spectrum of Fe 2p for the o-Fe/NC.

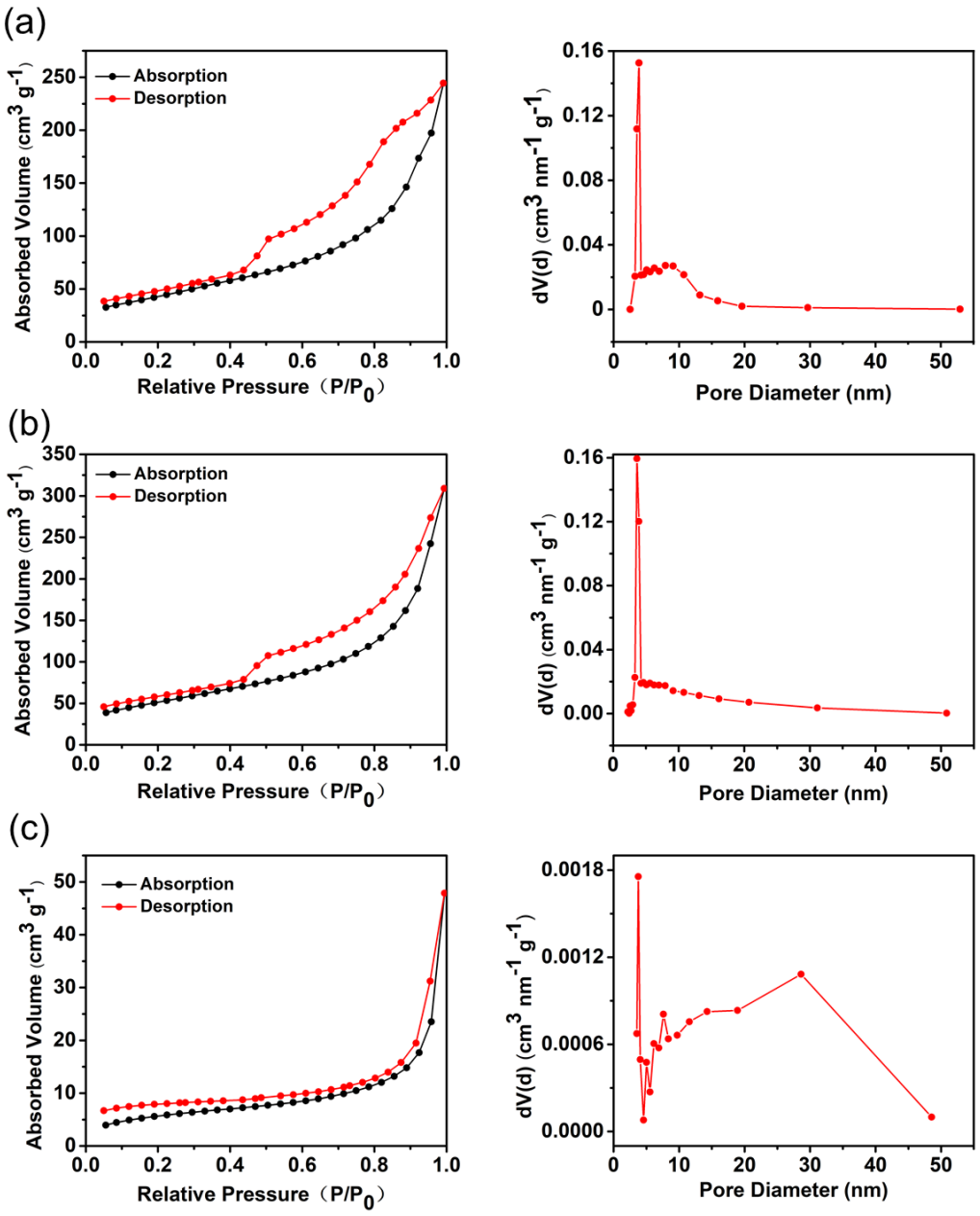

Figure S8. N_2 adsorption and desorption isotherms and the pore size distribution curves of (a) o-Fe MOF, (b) o-Fe/NC and (c) m-Fe/NC.

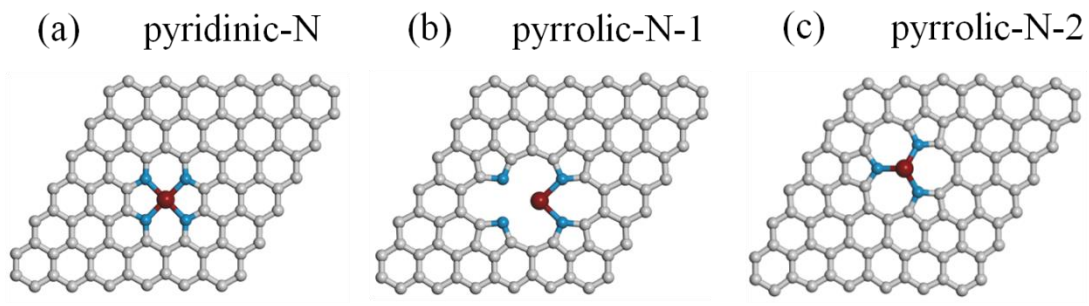

Figure S9. Geometric models of Fe atom coordinated with (a) pyridinic-N, (b,c) pyrrolic-N.

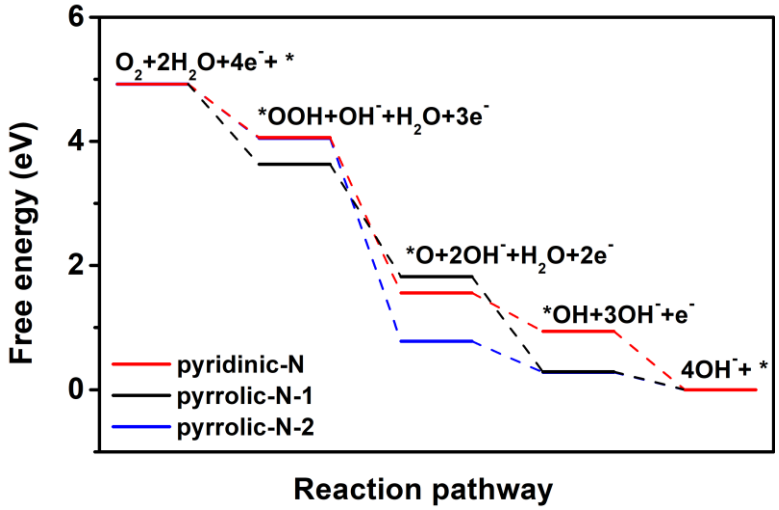

Figure S10. Free energy diagrams of oxygen reduction reaction processes for models of pyridinic-N, pyrrolic-N-1 and pyrrolic-N-2.

Table S1. The change in Gibbs free energy (ΔG) of each oxygen reduction reaction (ORR) step on surface of pyridinic-N, pyrrolic-N-1 and pyrrolic-N-2.

Step	pyridinic-N	pyrrolic-N-1	pyrrolic-N-2
$* + O_2\,(g) + H^+ + e^- \rightarrow *OOH$	-0.86	-1.29	-0.87
$*OOH + H^+ + e^- \rightarrow *O + H_2O(l)$	-2.50	-1.81	-3.27
$*O + H^+ + e^- \rightarrow *OH$	-0.62	-1.53	-0.50
$*OH + H^+ + e^- \rightarrow H_2O(l) + *$	-0.94	-0.29	-0.28

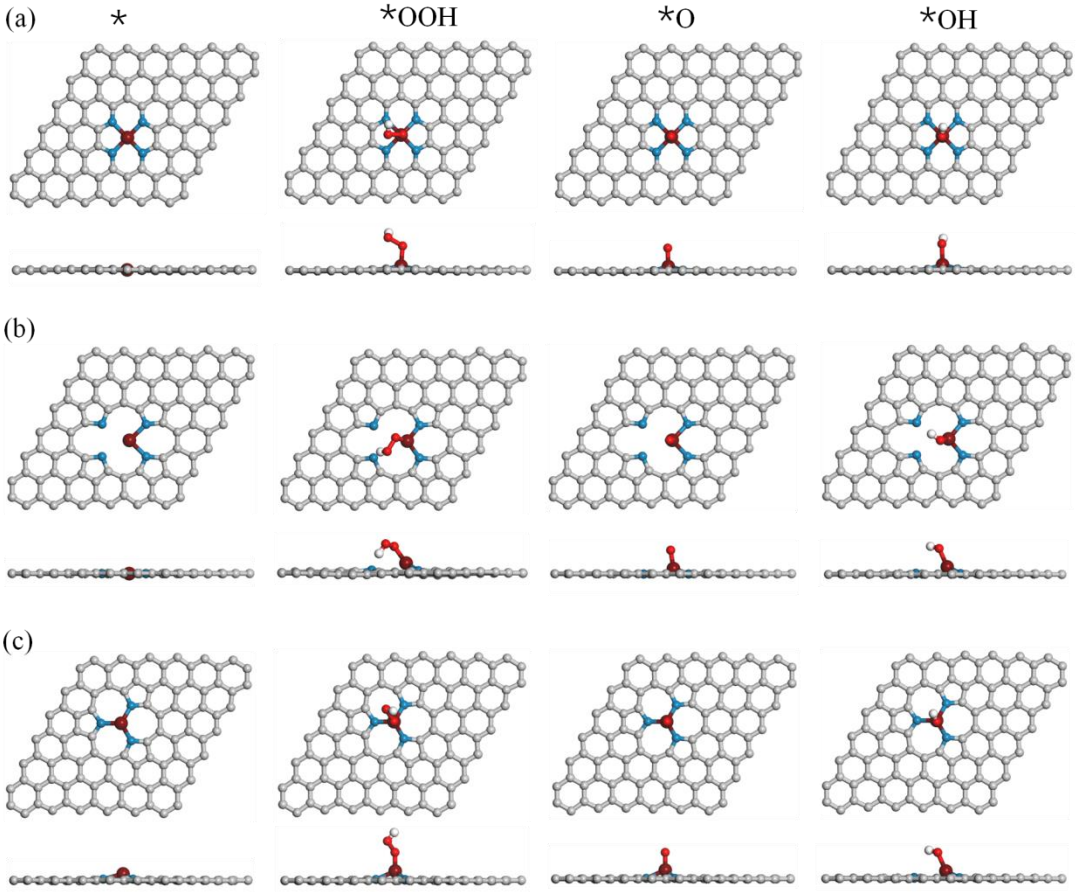

Figure S11. Geometric structures of Fe atom coordinated with (a) pyridinic-N, (b) pyrrolic-N-1, (c) pyrrolic-N-2, and the intermediates *OOH, *O, and *OH for ORR.

3. References

(1) G. Kresse, J. Furthmiiller, *Comput. Mater. Sci.*, 1996, **6**, 15-50.

(2) J. P. Perdew, K. Burke, M. Ernzerhof, *Phy. Rev. Lett.*, 1996, **78**, 3865-3868.

(3) P. E. Blochl, *Phys. Rev. B*, 1994, **50**, 17953-17979.

(4) J. K. Nørskov, J. Rossmeisl, A. Logadottir, L. Lindqvist, J. R. Kitchin, T. Bligaard, H. Jonsson, *Phys. Chem. B*, 2004, **108**, 17886-17892.

(5) H. Monkhorst, J. Pack, *Phys. Rev. B*, 1976, **13**, 5188-5192.